

# Investigation of carbon steel anodic dissolution in ammonium chloride solutions using electrochemical impedance spectroscopy

Prince Kumar Baranwal<sup>1</sup> · R. Prasanna Venkatesh<sup>1</sup>

Received: 6 September 2016 / Revised: 4 December 2016 / Accepted: 26 December 2016 / Published online: 7 January 2017  
© Springer-Verlag Berlin Heidelberg 2017

**Abstract** The anodic dissolution of carbon steel in ammonium chloride (NH<sub>4</sub>Cl) solutions (5, 10, and 20 wt%) is investigated via various electrochemical techniques and other complementary techniques. The polarization measurements reveals that the carbon steel is susceptible to general corrosion. The impedance data taken at various overpotentials shows multiple loops, corresponding to capacitance, inductance, and negative capacitance, and the number of time constants observed is also not the same for various NH<sub>4</sub>Cl concentrations. From reaction mechanism analysis, a multi-step reaction mechanism with three adsorbed intermediates and three dissolution paths (one chemical path and two electrochemical paths) is proposed to describe the observed patterns in impedance measurements. The surface coverage of intermediate species and the contribution of chemical reaction and electrochemical reaction to the overall corrosion rate are also estimated from the proposed model. The results obtained from field emission scanning electron microscopy and Raman spectroscopy measurements are also reported.

**Keywords** Carbon steel · Ammonium chloride · Electrochemical impedance spectroscopy · Reaction mechanism

**Electronic supplementary material** The online version of this article (doi:10.1007/s10008-016-3497-8) contains supplementary material, which is available to authorized users.

✉ R. Prasanna Venkatesh  
rprasanna@iitg.ernet.in

<sup>1</sup> Department of Chemical Engineering, Indian Institute of Technology Guwahati, Guwahati 781039, India

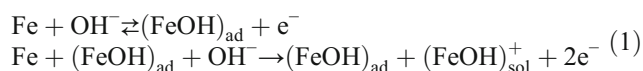
## Introduction

Corrosion by means of wet ammonium chloride salts or aqueous solutions of ammonium chloride (NH<sub>4</sub>Cl) has plagued the oil refining and petrochemical industries for many years. With processes and streams where nitrogen and chlorides or ammonia (NH<sub>3</sub>) and hydrochloric acid (HCl) are present, the formation of ammonium chloride is feasible. The ammonium chloride deposits leads to severe failure or corrosion as reported in the literature [1, 2]. The corrosivity of the NH<sub>4</sub>Cl stream depends on various factors such as concentration of NH<sub>4</sub>Cl, hydrodynamic conditions, temperature, etc.

Toba et al. [3] studied the effect of relative humidity and concentration of NH<sub>4</sub>Cl on carbon steel corrosion via weight loss and water absorption tests. The corrosion of various alloys in ammonium chloride solution was investigated, and the results show that the nature of corrosion (general corrosion or pitting corrosion) and the corrosion rate strongly depends upon the alloy composition [4]. The corrosion rate is also correlated to pitting resistant equivalent number (PREN) number which is estimated from alloy composition [5]. The effect of temperature and NH<sub>4</sub>Cl concentration was also characterized using polarization measurements, and the results show that both the parameters had a pronounced effect on the corrosion rate [4]. The composition of the corrosion product analyzed via thermogravimetric analysis (TGA) and spectroscopic studies reveals that the corrosion product contains a mixture of oxides and oxy-hydroxides [6, 7].

The reaction mechanism of carbon steel anodic dissolution in various media is extensively studied. Some of the important models which are reported in literature are summarized here: Heusler [8] proposed a two-step catalytic dissolution for acidic medium in which

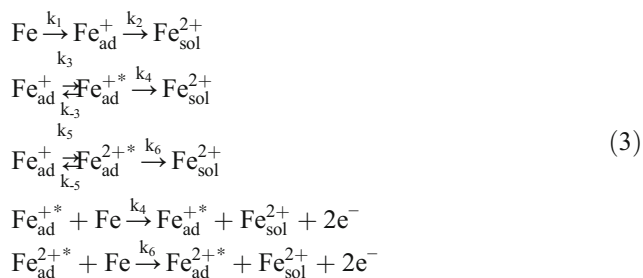
(FeOH)<sub>ad</sub> is an intermediate adsorbate but not consumed in the reaction.



The research group of Bockris [9–11] suggested a mechanism in which the dissolution of (FeOH)<sub>ad</sub> is considered to be slow.



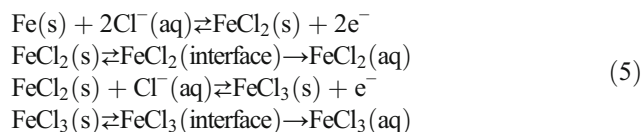
In both of the above models, the dissolution of Fe in the presence of only OH<sup>-</sup> ions was considered. Besides, if the impedance measurements show more than one time constant in addition to electrical double layer (EDL), then it is difficult to suggest the above models as it includes only one intermediate adsorbed species Fe(OH)<sub>ad</sub>. The effects of various ions in the electrolyte media on Fe dissolution behavior were also considered later. Keddama et al. [12] showed multi-step mechanism for Fe dissolution behavior in acidic media in the presence of sulfate ions with three adsorbed species (Fe<sub>ad</sub><sup>+</sup>, Fe<sub>ad</sub><sup>+\*</sup>, Fe<sub>ad</sub><sup>2+\*</sup>) as shown here:



They also added the following passivation step in the above mechanism to describe the pre-passivation behavior observed in polarization measurements.



Similarly, the corrosion of carbon steel in chloride media is also extensively investigated. The most widely accepted mechanism is proposed by Li and his coworkers [13] which is given below.



Although the carbon steel dissolution is extensively reported for various other chloride media, viz. NaCl and HCl, only few works were reported in the literature in respect to the anodic dissolution of carbon steel in ammonium chloride solutions. Especially, the mechanistic reaction pathway of corrosion of

carbon steel in NH<sub>4</sub>Cl solution is not exploited yet to the best of author's knowledge. Thus, proposing a kinetic model to describe the carbon steel anodic dissolution behavior in NH<sub>4</sub>Cl concentrations is of great interest in the present work.

Electrochemical impedance spectroscopy (EIS) is one of the powerful tools available for investigation of electrochemical and corrosion reaction mechanisms [14–18]. Various processes such as faradaic and non-faradaic reactions including adsorption–desorption, diffusion of chemical compounds/ions, and passivity of surfaces can be easily detected by means of EIS technique. With application of a small sinusoidal perturbation, electrode properties and other physical properties can be determined without interfering the system.

The reaction mechanism of metal dissolution in various medium is successfully investigated by EIS measurements [12, 19–21]. Keddama et al. [12], in particular, employed an approach called reaction mechanism analysis (RMA) to understand the anodic dissolution of metal in the solution through impedance data. Proposing/eliminating a mechanism based on the patterns observed in EIS measurements is possible. For example, a direct dissolution shows only single time constant in the impedance data while the dissolution through one intermediate species shows either single or double time constants depending on the parameter values. The various patterns that are possible for the given mechanism are summarized in the literature [21].

Hence, in this present work, EIS measurements were implemented besides polarization measurements, field emission scanning electron microscopy (FESEM) measurements, and Raman spectroscopy measurements to investigate the carbon steel anodic dissolution behavior in 5, 10, and 20 wt% NH<sub>4</sub>Cl solutions at room temperature. The RMA approach is employed to analyze the data obtained from EIS measurements.

## Experimental

### Materials

Carbon steel [C (0.22–0.26)%; Si (0.11–0.14)%; Mn (1.03–1.06)%; P (0.04 % maximum); S (0.03 % maximum); Cr (0.03 % maximum); and rest Fe] was used for all the measurements in this present work. NH<sub>4</sub>Cl (HiMedia) and Millipore water were used to prepare solutions of various concentrations (5, 10, and 20 wt%). All the experiments were carried out at natural pH of the solutions. The pH values of the solutions observed were 4.84, 4.69, and 4.22, respectively, for 5, 10, and 20 wt% NH<sub>4</sub>Cl solutions.

### Electrochemical measurements

Electrochemical experiments were conducted using a potentiostat [Metrohm Autolab, PGSTAT 204], and a standard

three electrode system, at  $(25 \pm 1)^\circ\text{C}$ . The working electrode fabricated with carbon steel of dia. 9 mm was implanted inside a Teflon tube, such that only the cross section interacts with the electrolytic solution. The reference electrode was made of Ag/AgCl (3 M KCl), and a Pt wire was used as the counter electrode. The corrosion cell was retained within a Faraday shield during all the experiments, in order to reduce the external perturbations from the surroundings. Prior to each experiment, the working electrode was smoothed sequentially with 180, 320, and 600 grades of emery paper, followed by 1.0 and  $0.3\ \mu\text{m}$  abrasive powder (alumina). The electrode was then washed with Millipore water and further ultrasonicated to eliminate any adhered particles. The polarization and impedance measurements were carried out only after the open circuit potential (OCP) reached the stable value. The polarization measurements were performed by sweeping the potential from OCP to +500 mV (w.r.t. OCP) to obtain the anodic branch, at a scan rate of  $1\ \text{mV s}^{-1}$ . The impedance measurements were performed by applying an amplitude of 10 mV (rms) for various dc potential (+0.05, +0.15, and +0.25 V w.r.t. OCP). The frequency range employed was from 100 kHz to 1 mHz, with six frequencies per decade. All the experiments were carried out at least twice, and only the repeatable results are presented in this work. All the measurements were conducted at static conditions using naturally aerated electrolyte solutions.

### Field emission scanning electron microscopy measurements

The surface morphology images of carbon steel were observed using field emission scanning electron microscope (Zeiss, Sigma), in order to characterize the type of corrosion. The carbon steel sample was submerged in nitric acid, followed by rinsing with water and polishing with emery paper and abrasive alumina powder. After polishing, the sample was rinsed with Millipore water, ultrasonicated, and air dried. The sample was then submerged in the respective solutions for a particular time period. At the end of 12 h, the sample was removed out of the system and rinsed with Millipore water. The washed sample was then air dried, and finally, the images were taken.

### Raman spectroscopy measurements

The corrosion products were analyzed using micro-Raman spectroscopy (Horiba Jobin Vyon, LabRam HR) in order to identify the type of iron oxide (corrosion product) formed on the carbon steel surface. The carbon steel sample was submerged in nitric acid, rinsed with water, followed by polishing with emery paper, and rinsed with Millipore water. The washed sample was then air dried and dipped in the respective solution. After 72 h, the sample was removed out of the system. The corrosion product formed was then scrubbed out,

dried in vacuum, and characterized using Raman spectroscopy with an excitation wavelength of 633 nm. The Raman spectra were recorded over a range of 100 to  $2000\ \text{cm}^{-1}$ .

## Results and discussion

### OCP and potentiodynamic polarization measurements

Prior to potentiodynamic polarization measurements, OCP measurements were carried out for a period of 300 s. The OCP values obtained for 5, 10, and 20 wt%  $\text{NH}_4\text{Cl}$  solutions are  $-0.710$ ,  $-0.706$ , and  $-0.686\ \text{V}$  [vs. Ag/AgCl (3 M KCl)], respectively. As OCP reaches the stable value within 300 s, the same is set as equilibration time for further electrochemical experiments. Figure 1 shows the anodic polarization curves of carbon steel in 5, 10, and 20 wt%  $\text{NH}_4\text{Cl}$  solutions respectively. The result shows that with an increase in concentration, the corrosion potential ( $E_{\text{corr}}$ ) shifts towards more positive values, though not significantly. Similar trend is also reported in the literature [4]. Also, the anodic current increases with an increase in  $\text{NH}_4\text{Cl}$  concentration as the anodic branches move towards the right. This reveals that the dissolution rate increases with an increase in ammonium chloride concentration.

The other observation in the polarization curves is the appearance of kink in the anodic branch which is more evident especially at higher concentrations of  $\text{NH}_4\text{Cl}$  (10 and 20 wt%). It could be expected that it might be due to the occurrence of pitting corrosion on the carbon steel surface, and the potential below which passivation occurs is referred as breakdown or pitting potential ( $E_b$ ). However, the following features, which are usually observed in polarization curve when pitting corrosion occurs, are not seen here [22–24]: (1) constant current with an increase in potential (formation of strong passive layer), (2) the sharp increase in current with a slight increase in the potential (breakdown of

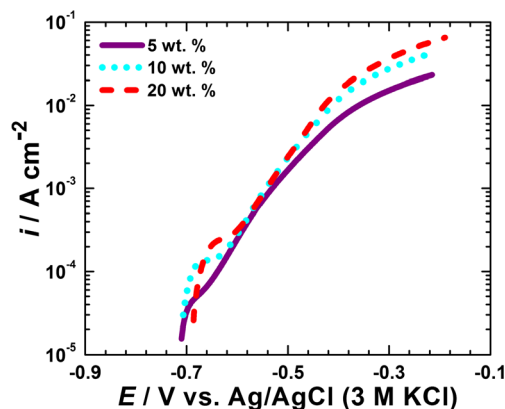


**Fig. 1** Anodic polarization curves of carbon steel corroded in 5, 10, and 20 wt%  $\text{NH}_4\text{Cl}$  solutions. Scan rate =  $1\ \text{mV s}^{-1}$

passive layer and formation of stable pits), and (3) a decrease of  $E_b$  and  $E_{\text{corr}}$  with an increase in  $\text{Cl}^-$  ion concentration. In the present case, constant current regime is observed only for the few millivolt ranges and the increase in current with potential after the  $E_b$  is more or less linear. This suggests that the corrosion observed is of general type although carbon steel is susceptible to pitting corrosion in chloride medium [25–27]. Especially, when the rate of general corrosion via hydroxyl groups is more compared to that of the rate of pitting corrosion via chloride ions, it is attributed to the thinning of oxide/hydroxide layer [28]. When this layer is thin and non-protective, one may expect the corrosion is of only general type. As the anodic polarization curve does not show any strong passivation, the corrosion may be of general type for the present system. It is also observed that corrosion is of either general type or pitting type depending on the composition of the alloy in the chloride media [4, 6]. In particular, it is reported that carbon steel undergoes general corrosion in ammonium chloride solutions [4].

### FESEM measurements

To confirm the type of corrosion, the surface morphology images of carbon steel were obtained using FESEM, with and without treatment in various concentrations of  $\text{NH}_4\text{Cl}$ .

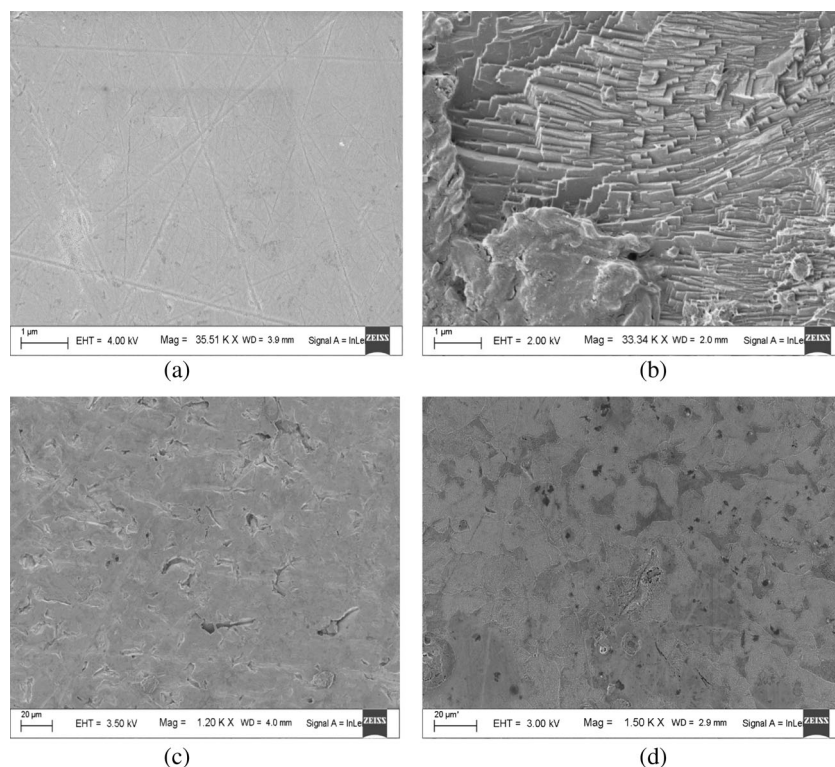
The results are shown in Fig. 2a–d. There were no corrosion marks as expected on untreated carbon steel sample. The carbon steel in various  $\text{NH}_4\text{Cl}$  concentrations (5, 10, and 20 wt%) shows that corrosion is more of uniform type as shown in Fig. 2b–d. It supports our presumption made from potentiodynamic polarization studies that general corrosion occurs when carbon steel of given composition reacts with  $\text{NH}_4\text{Cl}$  solution.

### Electrochemical impedance spectroscopy measurements

To understand the anodic dissolution behavior of carbon steel in different concentrations of  $\text{NH}_4\text{Cl}$ , EIS measurements were conducted at various dc potentials, i.e., +0.05, +0.15, and +0.25 V w.r.t. OCP, and the results are presented in Fig. 3a–i. The absolute potential indicated in these figures referred to the value of reversible hydrogen electrode (RHE). The EIS measurements were performed after the system reaches its stable OCP value.

Following observations were made based on the EIS data: (i) for 5 wt%  $\text{NH}_4\text{Cl}$  solution, the data shows three time constants for all the overpotentials investigated; (ii) for both 10 and 20 wt%  $\text{NH}_4\text{Cl}$  solutions, three time constants were observed at 0.05 and 0.15 V above OCP, while four time constants were observed at 0.25 V above OCP; (iii) the overall impedance decreases with overpotential for all the three concentrations, indicating that dissolution rate

**Fig. 2** FESEM images of **a** untreated carbon steel, **b** carbon steel after immersed in 5 wt%  $\text{NH}_4\text{Cl}$  solution for 12 h, **c** carbon steel after immersed in 10 wt%  $\text{NH}_4\text{Cl}$  solution for 12 h, and **d** carbon steel after immersed in 20 wt%  $\text{NH}_4\text{Cl}$  solution for 12 h





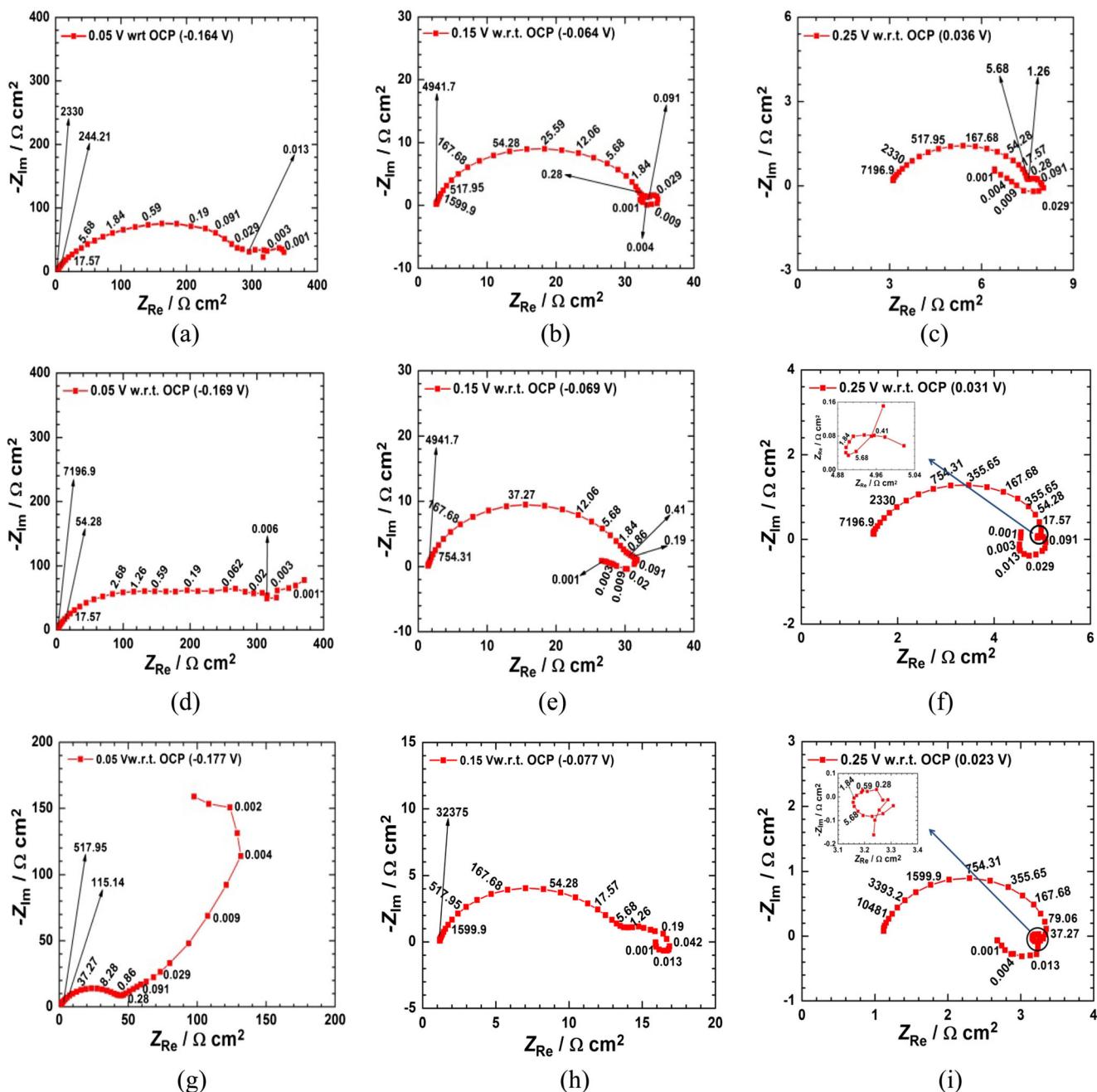


**Fig. 3** EIS measurement of carbon steel at various overpotentials in **a–c** 5 wt%  $\text{NH}_4\text{Cl}$  solution, **d–f** 10 wt%  $\text{NH}_4\text{Cl}$  solution, and **g–i** 20 wt%  $\text{NH}_4\text{Cl}$  solution. Frequency given is in hertz. The absolute potentials referred in the figures are w.r.t. RHE

increases with overpotential; and (iv) the overall impedance at any overpotential decreases with an increase in the concentration of  $\text{NH}_4\text{Cl}$ , indicating that dissolution rate increases with concentration as observed in polarization measurements. The loops at higher frequency are attributed to the EDL at metal–solution interface, while those at the mid and low frequencies would arise from faradaic and non-faradaic processes. It is also to be noted that with an increase in overpotential, the patterns keep on changing with an increase in the number of time constants from three

to four especially for 10 and 20 wt%  $\text{NH}_4\text{Cl}$  concentration. For 5 wt%  $\text{NH}_4\text{Cl}$ , three capacitance loops were observed at 0.05 V above OCP, while the low frequency capacitive loop is transformed into inductive loop for higher overpotentials. For 10 and 20 wt%  $\text{NH}_4\text{Cl}$  solutions, two capacitance loops in the higher and mid frequency regime and one inductance loop in low frequency regime are observed at 0.15 V above OCP. However, at 0.25 V above OCP, the number of time constants increased to four loops (capacitance–inductance–capacitance–inductance). At

0.05 V above OCP, three capacitance loops are observed for 10 wt% NH<sub>4</sub>Cl solution, while a negative capacitance is observed in the low frequency regime for 20 wt% NH<sub>4</sub>Cl solution. Most of the systems exhibit only a change in impedance with the patterns remaining the same when the overpotential is varied [19, 20, 29]. However, the change in observed patterns with a change in overpotential is also reported for some systems [13, 30].

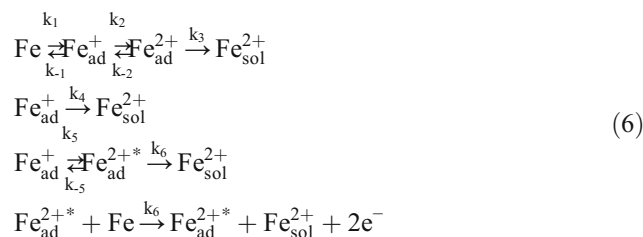
The EIS data obtained here is validated with Kramers-Kronig transform (KKT) to ensure the linearity, stability, and causality of the system [31–33]. The transformed data maps well with the experimental results (not shown here). As the EIS data shows different patterns at different overpotentials, as well as the number of time constants are increased to four at higher overpotentials, it is difficult to analyze all the experimental observations via electrical equivalent circuit (EEC) modeling approach which is commonly employed by many researchers [13, 34–36]. Thus, in this present work, a RMA approach is employed to describe the process occurring at metal–solution interface for all the concentrations through the obtained EIS data.

### Reaction mechanism analysis

In RMA, a reaction mechanism is propounded based on the experimental observations. The impedance data is then simulated for the considered mechanism and correlated with the experimental impedance data, especially with respect to the patterns obtained [15, 19–21]. For the systems being studied, a maximum of three time constants are observed besides a capacitive loop, which corresponds to EDL. Thus, a mechanism with at least three intermediate adsorbed species should be propounded to capture the experimental observations. Keddiam et al. [12] proposed a kinetic model with four intermediate adsorbed species to capture the four time constants. Recently, Fasmin et al. [37] suggested a mechanism for Ti dissolution in HF medium with two intermediate species to capture the three time constants. Thus, mechanisms such as direct dissolution and those involving one or two adsorbed intermediate species were discarded in the present work.

Samide et al. [6] reported from Mossbauer spectrometry studies that the main corrosion product of carbon steel dissolution in 0.1 M NH<sub>4</sub>Cl is a mixture of ferri(III)hydrite and Fe(III)oxide-hydroxide. Also, X-ray photoelectron spectroscopy (XPS) and thermogravimetric analysis (TGA) of corroded products of carbon steel in 1 M NH<sub>4</sub>Cl solution show that the dissolution species is more likely of Fe<sup>3+</sup> [7]. However, Fe<sup>2+</sup> is more thermodynamically stable in the existing pH value of the given system. Thus, in the present work, we

suggested the following mechanisms with Fe<sup>2+</sup> as dissolution species:



where Fe<sub>ad</sub><sup>+</sup> and Fe<sub>ad</sub><sup>2+</sup> correspond to adsorbed metal species, while Fe<sub>sol</sub><sup>2+</sup> corresponds to metal ion dissolved in solution. Fe<sub>ad</sub><sup>2+\*</sup> represents the intermediate adsorbed species but also acts as a catalyst for the step k<sub>6</sub>.

Though this mechanism is more similar to Keddiam et al. model [12], here we considered only three adsorbed species Fe<sub>ad</sub><sup>+</sup>, Fe<sub>ad</sub><sup>2+</sup>, and Fe<sub>ad</sub><sup>2+\*</sup> instead of four adsorbed species Fe<sub>ad</sub><sup>+</sup>, Fe<sub>ad</sub><sup>+</sup>, Fe<sub>ad</sub><sup>2+</sup>, and Fe<sub>ad</sub><sup>2+\*</sup>. Also, the pre-passivation due to Fe<sub>ad</sub><sup>2+</sup> is neglected as polarization measurements did not show any pre-passivation behavior in the investigated potential range.

Three dissolution paths via k<sub>3</sub>, k<sub>4</sub>, and k<sub>6</sub> are considered in this mechanism. Fe<sub>ad</sub><sup>+</sup> may be present as unstable metal ion complex with oxidation state +1, and Fe<sub>ad</sub><sup>2+</sup> may exist as oxide and hydroxide of Fe with oxidation state +2 on the carbon steel surface. However, the film is non-protective in nature and does not completely passivate the surface. Fe<sub>ad</sub><sup>2+</sup> may also exist in the form of ferrous chloride as chloride ions are present in the solution. The existence of oxides/oxy-hydroxides with Cl atoms inclusion is also possible.

The following assumptions were incorporated in the development of impedance equations for the proposed mechanism: (i) linear perturbation is applied using ac voltage signal of small amplitude, i.e., 10 mv (rms), so that only linear terms are considered in the equations; (ii) the kinetic parameters are exponentially proportional to the voltage, and the forward reaction has a positive exponent and the reverse equation has a negative exponent; and (iii) surface coverage is restrained to unity, employing Langmuir adsorption isotherm model to the adsorption of charged species on the surface. It is to be noted that consideration of other adsorption models would not lead to any additional time constant but could match the experimental data quantitatively better [12].

In the proposed mechanism, the k<sub>3</sub> step is a chemical reaction and is independent of voltage while the rest of steps are electrochemical reactions. The details regarding the derivation of impedance equation for the given reaction scheme have been presented well in the literature [15, 21, 37–39], and only the important steps for the proposed mechanism are summarized below.

The unsteady-state mass balance equation for the proposed mechanism, corresponding to the adsorbed species, gives,

$$\tau \frac{d\theta_1}{dt} = k_1(1-\theta_1-\theta_2-\theta_3) - k_2\theta_1 - k_4\theta_1 - k_5\theta_1 - k_{-1}\theta_1 + k_{-2}\theta_2 + k_{-5}\theta_3 \tag{7}$$

$$\tau \frac{d\theta_2}{dt} = k_2\theta_1 - k_3\theta_2 - k_{-2}\theta_2 \tag{8}$$

$$\tau \frac{d\theta_3}{dt} = k_5\theta_1 - k_{-5}\theta_3 \tag{9}$$

where  $\tau$  refers to the total number of sites available per unit area;  $\theta_1$ ,  $\theta_2$ , and  $\theta_3$  refer respectively the surface coverage of adsorbed species  $\text{Fe}_{\text{ad}}^+$ ,  $\text{Fe}_{\text{ad}}^{2+}$ , and  $\text{Fe}_{\text{ad}}^{2+*}$ ; and  $(1 - \theta_1 - \theta_2 - \theta_3)$  refers the vacant sites available.  $k_1, k_{-1}, k_2, k_{-2}, k_3, k_4, k_5, k_{-5}$ , and  $k_6$  are the rate constants for the corresponding steps, given generally as,

$$k_i = k_{i0}e^{b_iV} \tag{10}$$

where  $i = (1 \text{ to } 6)$  for forward reactions, and  $i = (-1 \text{ to } -5)$  for backward reactions.  $V$  is the overpotential.

Here,

$$b_i = \pm \frac{\alpha nF}{RT} \tag{11}$$

where  $\alpha$  is referred as transfer coefficient, having values within 0 and 1;  $n$  is the number of electrons involved in a rate determining step; and  $F, R$ , and  $T$  are respectively the faraday constant, the ideal gas constant, and the temperature. Value of  $b$  for forward reaction is considered as positive, while for reverse reaction, it is considered as non-positive. Under steady state conditions, we get,

$$k_1(1-\theta_{1ss}-\theta_{2ss}-\theta_{3ss}) + k_{-2}\theta_{2ss} + k_{-5}\theta_{3ss} = k_2\theta_{1ss} + k_4\theta_{1ss} + k_5\theta_{1ss} + k_{-1}\theta_{1ss} \tag{12}$$

$$k_2\theta_{1ss} = k_3\theta_{2ss} + k_{-2}\theta_{2ss} \tag{13}$$

$$k_5\theta_{1ss} = k_{-5}\theta_{3ss} \tag{14}$$

Here, all the rate constants are estimated at the dc potential (the potential w.r.t. OCP) where upon the impedance was measured. The subscript ss indicates the steady state. On solving the above three equations, the respective fractional steady-state surface coverage are found to be as,

$$\theta_{1ss} = \frac{k_1k_{-5}(k_3 + k_{-2})}{D} \tag{15}$$

$$\theta_{2ss} = \frac{k_1k_2k_{-5}}{D} \tag{16}$$

$$\theta_{3ss} = \frac{k_1k_5(k_3 + k_{-2})}{D} \tag{17}$$

where,

$$D = k_{-5}(k_3 + k_{-2})(k_1 + k_{-1} + k_2 + k_4 + k_5) - k_2k_{-5}(k_{-2} - k_1) - k_5(k_3 + k_{-2})(k_{-5} - k_1) \tag{18}$$

The unsteady-state current density is given by,

$$J = nF[k_1(1-\theta_1-\theta_2-\theta_3) + k_2\theta_1 + k_4\theta_1 + k_5\theta_1 + 2k_6\theta_3(1-\theta_1-\theta_2-\theta_3) - k_{-1}\theta_1 - k_{-2}\theta_2 - k_{-5}\theta_3] \tag{19}$$

Under steady-state conditions,

$$J_{ss} = nF[2k_3\theta_{2ss} + 2k_4\theta_{1ss} + 2k_6\theta_{3ss}(1-\theta_{1ss}-\theta_{2ss}-\theta_{3ss})] \tag{20}$$

The faradaic impedance is determined by differentiating Eq. (19) with respect to the voltage, given as,

$$\frac{dJ}{dV} = \left( Z_{F,m/s} \right)^{-1} = nF \left[ \frac{dk_1}{dV}(1-\theta_{1ss}-\theta_{2ss}-\theta_{3ss}) + k_1 \left( -\frac{d\theta_1}{dV} - \frac{d\theta_2}{dV} - \frac{d\theta_3}{dV} \right) + \frac{dk_2}{dV}\theta_{1ss} + k_2 \frac{d\theta_1}{dV} + \frac{dk_4}{dV}\theta_{1ss} + k_4 \frac{d\theta_1}{dV} + \frac{dk_5}{dV}\theta_{1ss} + k_5 \frac{d\theta_1}{dV} - \frac{dk_{-1}}{dV}\theta_{1ss} - k_{-1} \frac{d\theta_1}{dV} - \frac{dk_{-2}}{dV}\theta_{2ss} - k_{-2} \frac{d\theta_2}{dV} - \frac{dk_{-5}}{dV}\theta_{3ss} - k_{-5} \frac{d\theta_3}{dV} + 2 \frac{dk_6}{dV}\theta_{3ss}(1-\theta_{1ss}-\theta_{2ss}-\theta_{3ss}) + 2k_6 \left( \frac{d\theta_3}{dV} - \theta_{3ss} \frac{d\theta_1}{dV} - \theta_{1ss} \frac{d\theta_3}{dV} - \theta_{3ss} \frac{d\theta_2}{dV} - \theta_{2ss} \frac{d\theta_3}{dV} - 2\theta_{3ss} \frac{d\theta_3}{dV} \right) \right] \tag{21}$$

On rearrangement, we get,

$$\left( Z_{F,m/s} \right)^{-1} = R_t^{-1} - nF \left[ \frac{d\theta_1}{dV}(k_1 + k_{-1} - k_2 - k_4 - k_5 + 2k_6\theta_{3ss}) + \frac{d\theta_2}{dV}(k_1 + k_{-2} + 2k_6\theta_{3ss}) + \frac{d\theta_3}{dV}(k_1 - 2k_6 + 2k_6\theta_{1ss} + 2k_6\theta_{2ss} + 4k_6\theta_{3ss} + k_{-5}) \right] \tag{22}$$

where,

$$R_t^{-1} = nF \left[ (1-\theta_{1ss}-\theta_{2ss}-\theta_{3ss})(k_1b_1 + 2k_6b_6\theta_{3ss}) + (k_2b_2 + k_4b_4 + k_5b_5 - k_{-1}b_{-1})\theta_{1ss} - k_{-2}b_{-2}\theta_{2ss} - k_{-5}b_{-5}\theta_{3ss} \right] \tag{23}$$

Here,  $R_t$  indicates the charge transfer resistance.

$\frac{d\theta_1}{dV}$ ,  $\frac{d\theta_2}{dV}$ , and  $\frac{d\theta_3}{dV}$  values were attained by expanding mass balance equations using Taylor series and by neglecting higher order terms:

**Table 1** Best fit RMA parameters attained for carbon steel dissolution in different systems

Parameter	Values for various NH <sub>4</sub> Cl concentrations			Units
	5 wt%	10 wt%	20 wt%	
<i>R</i> <sub>sol</sub>	1.5	1.3	1.1	Ω cm <sup>2</sup>
<i>k</i> <sub>10</sub>	5.4 × 10 <sup>-10</sup>	6.4 × 10 <sup>-10</sup>	1.5 × 10 <sup>-9</sup>	mol s <sup>-1</sup> cm <sup>-2</sup>
<i>b</i> <sub>1</sub>	17	18.5	19	V <sup>-1</sup>
<i>k</i> <sub>-10</sub>	2.4 × 10 <sup>-6</sup>	6 × 10 <sup>-6</sup>	6 × 10 <sup>-6</sup>	mol s <sup>-1</sup> cm <sup>-2</sup>
<i>b</i> <sub>-1</sub>	0	0	0	V <sup>-1</sup>
<i>k</i> <sub>20</sub>	6.4 × 10 <sup>-7</sup>	1.3 × 10 <sup>-6</sup>	1.4 × 10 <sup>-6</sup>	mol s <sup>-1</sup> cm <sup>-2</sup>
<i>b</i> <sub>2</sub>	13	13	13	V <sup>-1</sup>
<i>k</i> <sub>-20</sub>	8 × 10 <sup>-6</sup>	1 × 10 <sup>-5</sup>	1 × 10 <sup>-5</sup>	mol s <sup>-1</sup> cm <sup>-2</sup>
<i>b</i> <sub>-2</sub>	-6	-6	-6	V <sup>-1</sup>
<i>k</i> <sub>30</sub>	4 × 10 <sup>-6</sup>	6.5 × 10 <sup>-6</sup>	6.5 × 10 <sup>-6</sup>	mol s <sup>-1</sup> cm <sup>-2</sup>
<i>b</i> <sub>3</sub>	0	0	0	V <sup>-1</sup>
<i>k</i> <sub>40</sub>	4 × 10 <sup>-8</sup>	5 × 10 <sup>-8</sup>	5 × 10 <sup>-8</sup>	mol s <sup>-1</sup> cm <sup>-2</sup>
<i>b</i> <sub>4</sub>	21	21	21	V <sup>-1</sup>
<i>k</i> <sub>50</sub>	2.4 × 10 <sup>-7</sup>	1 × 10 <sup>-6</sup>	2 × 10 <sup>-6</sup>	mol s <sup>-1</sup> cm <sup>-2</sup>
<i>b</i> <sub>5</sub>	3	1	1	V <sup>-1</sup>
<i>k</i> <sub>-50</sub>	8 × 10 <sup>-8</sup>	1 × 10 <sup>-7</sup>	1 × 10 <sup>-7</sup>	mol s <sup>-1</sup> cm <sup>-2</sup>
<i>b</i> <sub>-5</sub>	-5	-5	-5	V <sup>-1</sup>
<i>k</i> <sub>60</sub>	4 × 10 <sup>-9</sup>	2 × 10 <sup>-9</sup>	2 × 10 <sup>-9</sup>	mol s <sup>-1</sup> cm <sup>-2</sup>
<i>b</i> <sub>6</sub>	22	23	23	V <sup>-1</sup>
<i>Y</i> <sub>0</sub>	At OCP + 0.05 V	6 × 10 <sup>-5</sup>	6.2 × 10 <sup>-5</sup>	Ω <sup>-1</sup> cm <sup>-2</sup> s <sup>n</sup>
<i>n</i> <sub>1</sub>	At OCP + 0.05 V	0.9	0.91	
<i>Y</i> <sub>0</sub>	At OCP + 0.15 V	6.9 × 10 <sup>-5</sup>	7.8 × 10 <sup>-5</sup>	Ω <sup>-1</sup> cm <sup>-2</sup> s <sup>n</sup>
<i>n</i> <sub>1</sub>	At OCP + 0.15 V	0.92	0.93	
<i>Y</i> <sub>0</sub>	At OCP + 0.25 V	7.9 × 10 <sup>-5</sup>	8.1 × 10 <sup>-5</sup>	Ω <sup>-1</sup> cm <sup>-2</sup> s <sup>n</sup>
<i>n</i> <sub>1</sub>	At OCP + 0.25 V	0.95	0.97	
<i>τ</i>		2 × 10 <sup>-6</sup>	7 × 10 <sup>-6</sup>	mol cm <sup>-2</sup>

$$\frac{d\theta_1}{dV} = \frac{AF_1J_1 + BIG + CGJ_1}{D_1GJ_1 - AEJ_1 - BHG} \tag{24}$$

$$\frac{d\theta_2}{dV} = \frac{E\left(\frac{d\theta_1}{dV}\right) + F_1}{G} \tag{25}$$

$$\frac{d\theta_3}{dV} = \frac{H\left(\frac{d\theta_1}{dV}\right) + I}{J_1} \tag{26}$$

$$G = k_3 + k_{-2} + j\omega\tau$$

$$H = k_5$$

$$I = k_5(b_5 - b_{-5})\theta_{1ss}$$

$$J_1 = k_{-5} + j\omega\tau$$

The overall impedance of the system finally is given as,

$$Z_{total} = R_{sol} + \frac{1}{\left(\frac{Z_{F,m}}{s}\right)^{-1} + j\omega(Y_0)^{n_1}} \tag{27}$$

In the above equations,

$$n = 1$$

$$A = k_{-2} - k_1$$

$$B = k_{-5} - k_1$$

$$C = k_1b_1(1 - \theta_{1ss} - \theta_{2ss} - \theta_{3ss}) - (k_2b_2 + k_4b_4 + k_5b_5 + k_{-1}b_{-1})\theta_{1ss} + k_{-2}b_{-2}\theta_{2ss} + k_{-5}b_{-5}\theta_{3ss}$$

$$D_1 = k_1 + k_2 + k_4 + k_5 + k_{-1} + j\omega\tau$$

$$E = k_2$$

$$F_1 = k_3(b_2 - b_3)\theta_{2ss} + k_{-2}(b_2 - b_{-2})\theta_{2ss}$$

**Table 2** *R*<sub>t</sub> and CPE values estimated from RMA approach

NH <sub>4</sub> Cl conc. (wt%)	dc overpotential (V)	RMA	
		<i>R</i> <sub>t</sub> Ω cm <sup>2</sup>	<i>C</i> <sub>dl</sub> F cm <sup>-2</sup>
5	+0.05	312.5	2.1 × 10 <sup>-5</sup>
	+0.15	36.9	3.1 × 10 <sup>-5</sup>
	+0.25	3.6	4.8 × 10 <sup>-5</sup>
10	+0.05	250	2.3 × 10 <sup>-5</sup>
	+0.15	27.6	3.4 × 10 <sup>-5</sup>
	+0.25	2.6	5.8 × 10 <sup>-5</sup>
20	+0.05	97.1	2.4 × 10 <sup>-5</sup>
	+0.15	10.2	4.7 × 10 <sup>-5</sup>
	+0.25	1.1	6.6 × 10 <sup>-5</sup>



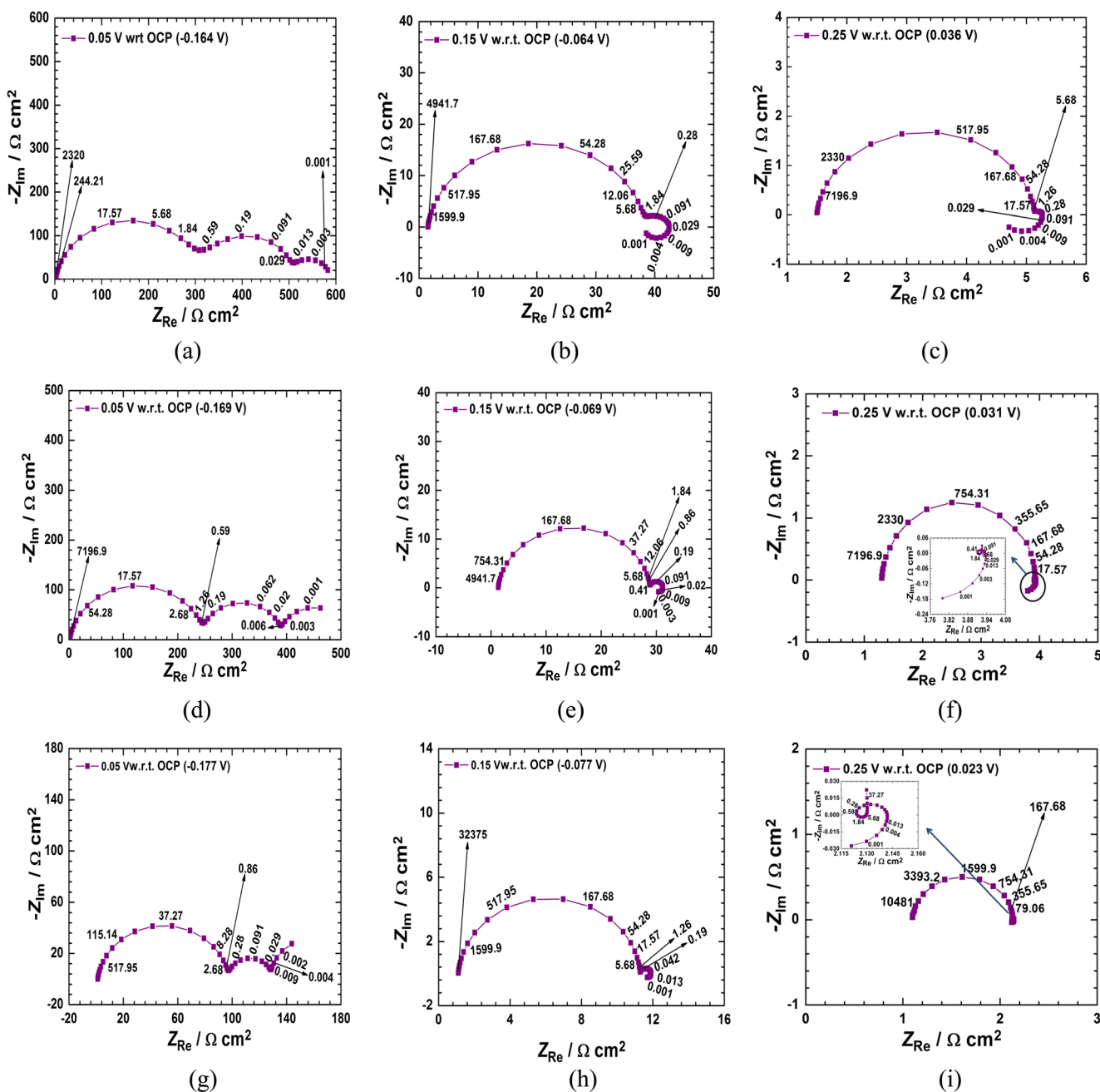


**Fig. 4** Simulated impedance values from RMA at various overpotentials for **a–c** 5 wt%  $\text{NH}_4\text{Cl}$  solution, **d–f** 10 wt%  $\text{NH}_4\text{Cl}$  solution, and **g–i** 20 wt%  $\text{NH}_4\text{Cl}$  solution. Frequency given is in hertz. The absolute potentials referred in the figures are w.r.t. RHE

Here,  $Y_0$ ,  $n_1$ , and  $R_{\text{sol}}$  respectively indicates the constant phase element (CPE) parameter, the exponent of CPE, and the solution resistance. The CPE parameters have been incorporated in the equation, as the EIS data shows a suppressed semicircle in the higher frequency region. The CPE values are analyzed with following Brug formula, in order to verify that the electrical double layer capacitance ( $C_{\text{dl}}$ ) values obtained are consistent with the literature and the estimated values are given in Table 2. Although different models were reported in the literature to calculate  $C_{\text{dl}}$  values from CPE components

[40, 41], we considered the following model with the assumption that system exhibits CPE behavior due to the variation of properties along the metal surface rather than on normal to the surface.

$$C_{\text{eff}} = \left[ Y_0 \left( \frac{1}{R_{\text{sol}}} + \frac{1}{R_{\text{ct}}} \right)^{n-1} \right]^{1/n} \tag{28}$$

An optimization technique, sequential quadratic programming (SQP), was used to obtain the RMA parameters, where

the code was written in MATLAB. The best fit RMA parameters were retrieved by reducing the subsequent residue term:

Residue

$$= \sum \left[ \omega_{\text{Re}} (Z_{\text{Reexperimental}} - Z_{\text{Rebestfit}})^2 + \omega_{\text{Im}} (Z_{\text{Imexperimental}} - Z_{\text{Imbestfit}})^2 \right] \quad (29)$$

where  $\omega_{\text{Re}}$  and  $\omega_{\text{Im}}$  are the weighing functions, considered as unity for RMA simulations. The best fit RMA parameters are given in Table 1 and the RMA simulated impedance patterns in Fig. 4a–i. Although our simulations show that the simulated impedance are more close to the experimental data at these particular parameter sets, the possibility of showing a similar match at other parameter values could not be discarded.

Although quantitative difference appears in impedance values between the experimental and the modeled data, the proposed kinetic model reproduces the observed patterns in the EIS data. Only the negative capacitance observed at 0.05 V w.r.t OCP for 20 wt%  $\text{NH}_4\text{Cl}$  concentration could not be captured by the proposed model. The remaining features such as decrease in impedance with overpotential for the given  $\text{NH}_4\text{Cl}$  concentration, decrease in impedance with  $\text{NH}_4\text{Cl}$  concentration at a given overpotential, and the number of time constants for the given overpotential and concentration are also well captured.

The surface coverage is estimated from these RMA parameters for the three adsorbed species. The results show that the surface coverage of both  $\text{Fe}_{\text{ad}}^+$  and  $\text{Fe}_{\text{ad}}^{2+}$  is negligible though they are increasing with concentration as well as with overpotential. It suggests that the formation and dissolution of these adsorbed species are more dynamic in nature. At any given overpotential and concentration, the surface is covered with mostly  $\text{Fe}_{\text{ad}}^{2+}$  species. The maximum surface coverage obtained is 0.26 for 20 wt%  $\text{NH}_4\text{Cl}$  concentration at 0.25 V above OCP as shown in Fig. 5. It suggests that the surface is not covered with thin film of oxide which would be the

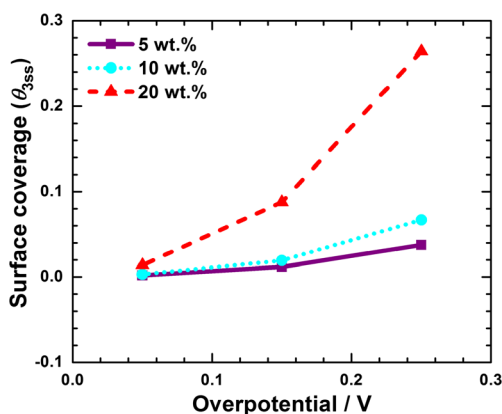


**Fig. 5** Surface coverage of  $\text{Fe}_{\text{ad}}^{2+}$  species as a function of dc overpotential for various concentrations of  $\text{NH}_4\text{Cl}$

possible reason for general corrosion. If the surface is covered with continuous oxide layer, then  $\text{Cl}^-$  ions might penetrate through the layer and induce pitting corrosion which is not the case here.

The dissolution rate via two dissolutions paths (chemical path and electrochemical path) is also estimated as a function of overpotential for various  $\text{NH}_4\text{Cl}$  concentrations, and the results are shown in Fig. 6. For all  $\text{NH}_4\text{Cl}$  concentrations, the dissolution via electrochemical step is predominant at higher overpotential while dissolution via chemical step is predominant at lower overpotential. It would be attributed to the increase in  $\theta_{3\text{ss}}$  value with overpotential for all  $\text{NH}_4\text{Cl}$  concentrations as the presence of  $\text{Fe}_{\text{ad}}^{2+}$  species facilitates the electrochemical dissolution via  $k_6$  step.

The values of  $C_{\text{dl}}$  estimated from  $Y_0$  and  $n_1$  and  $R_t$  values estimated using Eq. 23 are shown in Table 2. The exponent value of CPE ( $n_1$ ) is less than 1 in all the cases which might arise from the heterogeneities of the corroded surface [42–46]. The  $R_t$  values clearly show that the anodic dissolution rate increases with concentration of  $\text{NH}_4\text{Cl}$  at any given overpotential. It would be attributed to the increase of  $k_1$ ,  $k_2$ , and  $\tau$  values with concentration as the remaining rate constants are not changing at higher concentrations. The increase of dc current with an increase in dc potential as observed in polarization curves is also qualitatively captured by the suggested model. Consideration of additional steps in the kinetic model may require explaining the EIS data quantitatively better. However, the main aim of this present work is to propose a kinetic model with minimum number of parameters that could explain the carbon steel corrosion behavior adequately well.

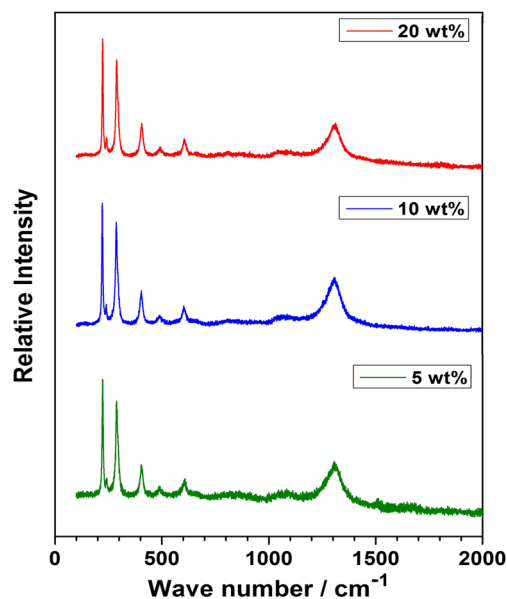


**Fig. 7** Raman spectra of the corrosion products obtained from carbon steel dissolution in 5, 10, and 20 wt%  $\text{NH}_4\text{Cl}$  solutions

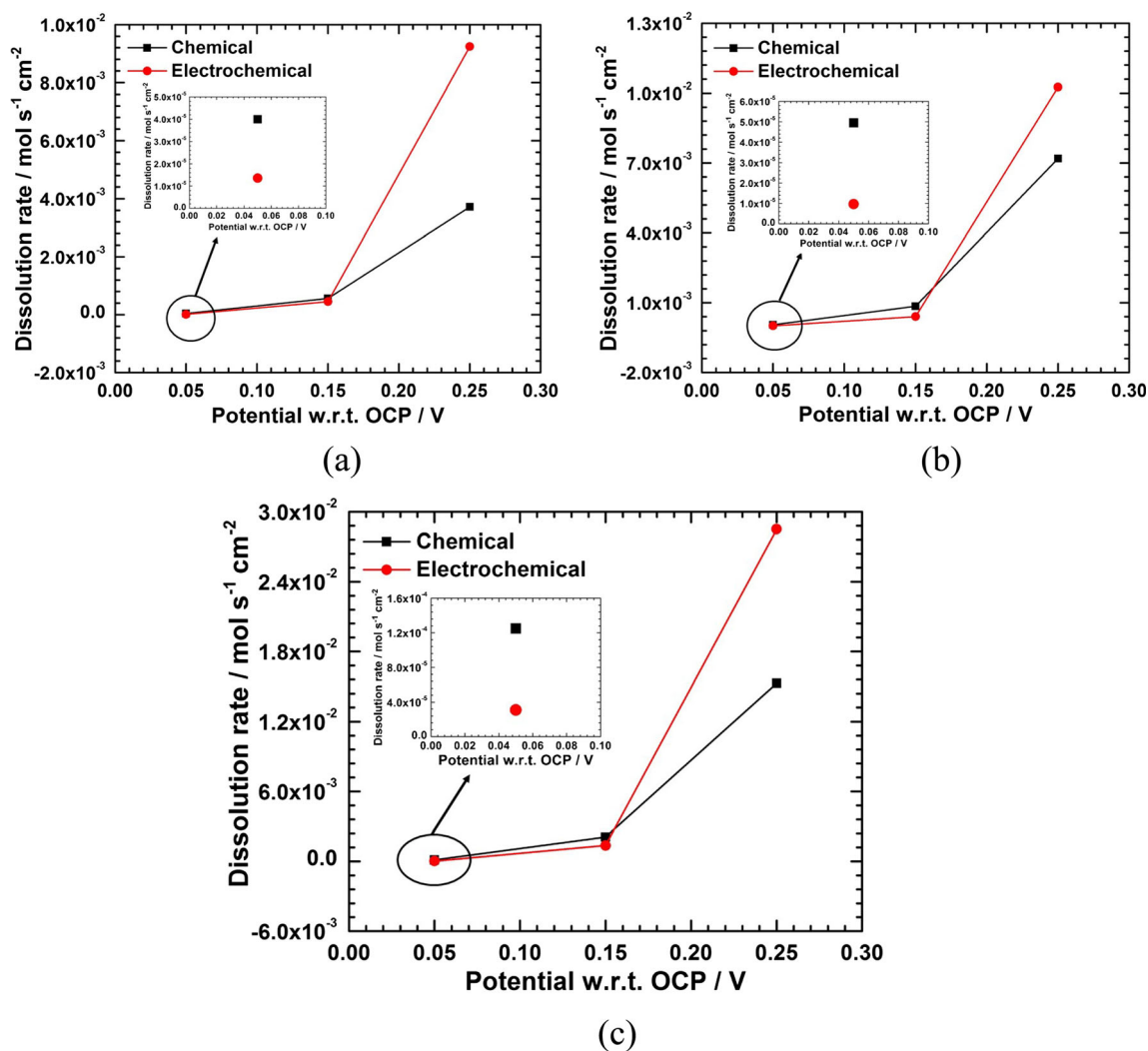


**Fig. 6** Contribution of chemical step and electrochemical step to dissolution rate at various overpotentials for **a** 5 wt%, **b** 10 wt%, and **c** 20 wt%  $\text{NH}_4\text{Cl}$  solutions

### Raman spectroscopy measurements

The corrosion products formed on the surface were analyzed using Raman spectroscopy measurements, and the recorded Raman spectra are shown in Fig. 7 for various concentrations of  $\text{NH}_4\text{Cl}$ . The spectra exhibit peaks at 223, 289, 404, 492, and 609  $\text{cm}^{-1}$  in addition to one shoulder peak at 245  $\text{cm}^{-1}$  for all  $\text{NH}_4\text{Cl}$  concentrations. All these peaks correspond to hematite ( $\alpha\text{-Fe}_2\text{O}_3$ ) [47, 48]. The peak observed at 1317  $\text{cm}^{-1}$  is shifted to lower wavenumber (1300  $\text{cm}^{-1}$ ) when the  $\text{NH}_4\text{Cl}$  concentration increases from 5 to 20 wt% which may be due to change in crystallinity or grain size of the corrosion product [49]. The existence of  $\gamma\text{-FeOOH}$  (lepidocrocite) in corrosion products could not be discarded as the Raman spectrum of the same exhibits peak at 1307  $\text{cm}^{-1}$ . Although the dissolution species is  $\text{Fe}^{2+}$ , it would be oxidized into  $\text{Fe}^{3+}$  due to the presence of dissolved oxygen in electrolyte solution. Other possible reason is oxidation of  $\text{Fe}^{2+}$  species due to the oxygen

present in air during sample preparation. Hence, in order to understand the reactions occurring at the carbon steel–electrolyte solution interface better and to support our observations made from our measurements, other relevant in situ methods such as electrochemical tunneling microscopy could be employed.

### Conclusion

The anodic dissolution of carbon steel in various  $\text{NH}_4\text{Cl}$  concentrations is investigated. The dissolution rate increases with an increase in  $\text{NH}_4\text{Cl}$  concentration within the range investigated. The polarization measurements reveal that general corrosion occurs on the surface. The surface morphology images of the carbon steel surface corroded with various  $\text{NH}_4\text{Cl}$  concentrations also confirms the same. EIS measurements were carried out at different overpotentials, and the results show a

maximum of four time constants at higher  $\text{NH}_4\text{Cl}$  concentrations while only three time constants were observed at 5 wt%  $\text{NH}_4\text{Cl}$ . Also, the patterns observed are changing with overpotential. Thus, a detailed reaction mechanism is employed to understand the dissolution behavior of carbon steel. The analysis shows that the dissolution occurs via three dissolution steps which involve both chemical and electrochemical paths, and the dissolved species is  $\text{Fe}^{2+}$ . The contribution of chemical reaction to the overall dissolution rate is significant at lower overpotential, while the contribution from electrochemical steps is significant at higher overpotential. Although the suggested model predicts the anodic dissolution behavior qualitatively well, consideration of additional steps may require to describe the EIS data quantitatively as well.

**Acknowledgements** This work was supported by DST-SERB, India (SERB/F/1365/2014-15). We acknowledge Central Instruments Facility of Indian Institute of Technology, Guwahati, India for providing facility for FESEM and Raman spectroscopy analysis.

## References

- Alvisi PP, Lins VDFC (2008) *Eng Fail Anal* 15:1035–1041
- Speight J (2015) *Fouling in refineries*. Elsevier Science and Technology, United Kingdom
- Toba K, Suzuki T, Kawano K, Sakai J (2011) *NACE Intl* 67: 0550051 (1-7)
- Toba K, Ueyama M, Kawano K, Sakai J (2012) *NACE Intl* 68: 1049–1056
- Forsen O, Aromaa J, Tavi M (1993) *Corros Sci* 35:297–301
- Samide A, Bibicu I, Rogalski MS, Preda M (2004) *J Radioanal Nucl Chem* 261:593–596
- Tutunaru B, Samide A, Negrila C (2013) *J Therm Anal Calorim* 111:1149–1154
- Heusler KE (1958) *Z Elektrochem* 62:582
- Bockris JOM, Drazic D, Despic AR (1961) *Electrochim Acta* 4: 325–361
- Bockris JOM, Kita H (1961) *J Electrochem Soc* 108:676–685
- Bockris JOM, Drazic D (1962) *Electrochim Acta* 7:293–313
- Keddum M, Mattos OR, Takenouti H (1981) *J Electrochem Soc* 128:257–266
- Li W, Nobe K, Pearlstein AJ (1990) *Corros Sci* 31:615–620
- Macdonald JR, Barsoukov E (2005) *Impedance spectroscopy: theory, experiment and applications*, 2nd edn. Wiley, New Jersey
- Orazem M, Tribollet B (2008) *Electrochemical impedance spectroscopy*. John Wiley and Sons, New Jersey
- Macdonald DD (2006) *Electrochim Acta* 51:1376–1388
- Zhang XG (1996) *Corrosion and electrochemistry of zinc*, 1st edn. Plenum, New York
- Bard AJ, Faulkner LR (2001) *Electrochemical methods: fundamentals and applications*, 2nd edn. John Wiley & Sons, New York
- Prasad YN, Kumar VV, Ramanathan S (2009) *J Solid State Electrochem* 13:1351–1359
- Venkatesh RP, Ramanathan S (2010) *J Appl Electrochem* 40:767–776
- Maddala J, Krishnaraj S, Kumar VV, Ramanathan S (2010) *J Electroanal Chem* 638:183–188
- Trueba M, Trasatti SP (2010) *Mater Chem Phys* 121:523–533
- Kuo HS, Chang H, Tsai WT (1999) *Corros Sci* 41:669–684
- McCafferty E (2010) *Introduction to corrosion science*, 1st edn. Springer, New York
- Cáceres L, Vargas T, Herrera L (2009) *Corros Sci* 51:971–978
- Lin B, Hu R, Ye C, Li Y, Lin C (2010) *Electrochim Acta* 55:6542–6545
- Mao X, Liu X, Revie RW (1994) *Corros Sci* 50:651–657
- Zaid B, Saidi D, Zaid AB, Hadji S (2008) *Corros Sci* 50:1841–1847
- Venkatesh RP, Ramanathan S (2010) *J Solid State Electrochem* 14: 2057–2064
- Strmčnik D, Gaberšček M, Pihlar B, Kočar D, Jamnik J (2009) *J Electrochem Soc* 156:C222–C229
- Agarwal P, Orazem ME (1995) *J Electrochem Soc* 142:4159–4168
- Boukamp BA (1995) *J Electrochem Soc* 142:1885–1894
- Macdonald MU, Real S, Macdonald DD (1986) *J Electrochem Soc* 133:2018–2024
- Lu J, Garland JE, Pettit CM, Babu SV, Roy D (2004) *J Electrochem Soc* 151(10):G717–G722
- Cho BJ, Venkatesh RP, Kwon TY, Park JG (2013) *Intl J Electrochem Sci* 8:4723–4734
- Freitas S, Malacarne MM, Romao W, Dalmaschio GP, Castro EVR, Celante VG, Freitas MBJG (2013) *Fuel* 104:656–663
- Fasmin F, Praveen BVS, Ramanathan S (2015) *J Electrochem Soc* 162(9):H604–H610
- Macdonald DD, Real S, Smedley SI (1988) *Urquidi-Macdonald. J Electrochem Soc* 135:2410–2414
- Bojinov M (1996) *J Electroanal Chem* 405:15–22
- Hirschorn B, Orazem ME, Tribollet B, Vivier V, Frateur I, Musiani M (2010) *Electrochim Acta* 55:6218–6227
- Germain PS, Pell WG, Conway BE (2004) *Electrochim Acta* 49: 1775–1788
- Sadkowsky A (2000) *J Electroanal Chem* 481:222–226
- Sadkowsky A (2000) *J Electroanal Chem* 481:232–236
- Pajkossy T (2005) *Solid State Ionics* 176:1997–2003
- Hirschorn B, Orazem ME, Tribollet B, Vivier V, Frateur I, Musiani M (2010) *J Electrochem Soc* 157:C452–C457
- Hirschorn B, Orazem ME, Tribollet B, Vivier V, Frateur I, Musiani M (2010) *J Electrochem Soc* 157:C458–C463
- Oh SJ, Cook DC, Townsend HE (1998) *Hyperfine Interact* 112:59–65
- Adhyapak PV, Mulik UP, Amalnerkar DP, Mulla IS (2013) *J Am Ceram Soc* 96(3):731–735
- Wang A, Haskin LA, Jolliff BL (1998) *Lunar Planet Sci Conf* 29